Peer-reviewed version available at Lubricants 2018, 6, 95; doi:10.3390/lubricants6040095

Article

About the accuracy and the grid convergence of the numerical solution of the energy equation in fluid film lubrication

Silun Zhang[1, 2], Mohamed-Amine Hassini[1] and Mihai Arghir[2,*]

[1] ERMES-IMSIA, EDF Lab Paris-Saclay, 91120 Palaiseau, France; mohamed-amine.hassini@edf.fr
[2] PPRIME Institute, UPR CNRS 3346, Université de Poitiers, ISAE ENSMA, 86962 Chasseneuil Futuroscope, France; silun.zhang@univ-poitiers.fr
* Correspondence: mihai.arghir@univ-poitiers.fr ; Tel.: +33(0)549496540

Abstract: The present work is focused on the numerical solution of the complete energy equation used in fluid film lubrication. The work was motivated by the fact the complete energy equation has no analytic solution that could be used for validations. Its accuracy and computation time are related to the employed numerical method and to the grid resolution. The natural discretization method (NDM) applied on different grids is systematically compared with the spectral method (the Lobatto Point Colocation Method or LPCM) with different polynomial degrees. A one dimensional inclined slider is used for the numerical tests and the energy equation is artificially decoupled from Reynolds. This approach enables to focus all the attention on the numerical solution of the energy equation. The results show that the LPCM is one or two orders of magnitudes more efficient than the NDM in terms of computation time. The energy equation is then coupled with Reynolds equation in a thermo-hydrodynamic analysis of the same 1D slider; the numerical results confirm again the efficiency of the LPCM. A thermo-hydrodynamic analysis of a two-lobe journal bearing is then presented as a practical application.

Keywords: energy equation; numerical solution; Lobatto point quadrature; Legendre polynomials

1. Introduction

The flow of thin lubricant films in journal and thrust bearings is most often described by the Reynolds equation of lubrication coupled with the energy transport equation. The numerical solution of these two-coupled equations is a problem solved since many decades [1]. However, it requires a computational effort that can render transient analyses very time consuming. Therefore, efficient solvers and adequate coupling strategies become of major importance to perform complex analyses in a reasonable amount of time.

If film rupture and reformation (traditionally designed as “cavitation”) are absent and if the flow regime is laminar and isothermal, then Reynolds equation is an elliptic linear differential equation. A direct solver can be used after its discretization in the thin film plane.

The energy equation contains convective transport terms, conductive transport terms across the thin film and dissipative source terms arising from its coupling with the Reynolds equation. Its character is therefore not entirely elliptic and its solver is different from the one used for the Reynolds equation. Moreover, the energy equation must be discretized also across the thin fluid film and the number of discretization points in that direction must be large enough to capture temperature gradients near the walls. Therefore, the energy equation requires a substantially higher computational effort compared to the Reynolds equation. Developing an accurate and efficient solver for the energy equation is then an important step toward solving non-isothermal lubrication problems. The task is not simple because there is no analytical solution of the complete energy equation to be used for validations. For example, if the analytical solution of the laminar and

isothermal thin film flow in a one dimensional (1D) slider can be used to validate the Reynolds equation solver, no similar solution exists for the energy equation. For validation, a numerical solver for the energy equation will have to be tested with different wall boundary conditions and the numerical results must be checked for various grid densities. Such results are absent from the literature.

As mentioned above, the energy equation must be discretized also across the film thickness. This renders its solution time consuming and the normal practice is to increase the number of discretization cells across the thin film until reaching a grid independent numerical solution. In natural discretization methods (NDM), such as finite difference or finite volumes methods, the variation of the temperature between two cells is linear. This leads to an important number of discretization cells across the thin film. An efficient approach for solving the energy equation was introduced by Elrod and uses the Legendre polynomials to describe the temperature variation across the thin film [2]. The coefficients of the Legendre polynomials expansion were first obtained by using a Galerkin approach. Later, Elrod used the collocation method at the Lobatto points, i.e. the roots of the derivative of the highest order of the used Legendre polynomial. This method known as the "Lobatto Points Collocation Method (LPCM)" proved to be more efficient [3].

Despite its efficiency, the method was barely used likely because of its complexity. Thus, Moraru [4] extended the LPCM to compressible films by describing the variation of the density across the thin film with Legendre polynomials. Feng and Kaneko [5] used the LPCM to solve the energy equation in aerodynamic foil bearings. Lehne et al [6] presented a comprehensive review of the numerical solution strategies of the coupled Reynolds and energy equations including the LPCM. Except for the cited references, the literature is scarce in references dealing with the LPCM.

This work presents a systematic comparison between the natural discretization method (NDM) of the energy equation and its LPCM approximation. In order to decouple Reynolds and energy equation, the viscosity is supposed to be constant and the flow laminar. A one dimensional (1D) inclined slider is used for the numerical tests. The Reynolds equation has then an analytical solution and the analysis is entirely focused on the energy equation. The results for the 1D slider compare both the number of points and the computational time required by the NDM and by the LPCM to obtain grid independent solutions. The results show how the NDM is excessively time consuming when high accuracy is sought and the net economy of computational time brought by the LPCM approach.

A thermo-hydrodynamic analyses of the 1D slider with coupled Reynolds and energy equation is then performed. The analyses highlight the same conclusions, namely the large superiority of the LPCM compared to NDM in terms of computational effort. Lastly, a two-lobe journal bearing with an axial supply groove is analyzed to demonstrate the accuracy that can be expected with simple, non-triggered boundary conditions for the energy equation.

2. The numerical solution of the energy equation based on the natural discretization method

This 1D inclined slider shown in **Figure 1** is used in [2] and [3] for the resolution of the Reynolds equation coupled with the energy equation. The current work is focused on the resolution of the energy equation decoupled from Reynolds equation for which an analytical solution is used. This gives an accurate numerical solution of the energy equation without the influence of the coupling with pressure and velocities affected by numerical uncertainties. The numerical data used is detailed in **Table 1**.

Preprints (www.preprints.org) | NOT PEER-REVIEWED | Posted: 14 September 2018 doi:10.20944/preprints201809.0251.v1

Peer-reviewed version available at Lubricants 2018, 6, 95; doi:10.3390/lubricants6040095

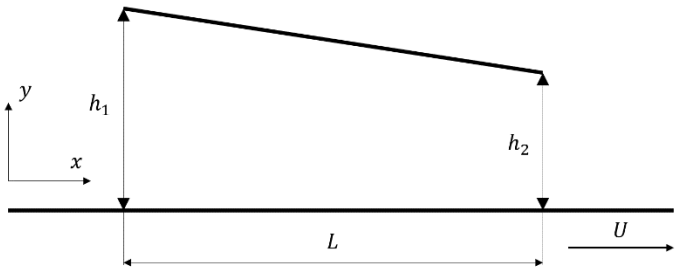

Figure 1. The 1D inclined slider

Table 1. The data used for the 1D slider

Density ρ_0	800 $[kg/m^3]$	Inlet thickness h_1	$1.8288e^{-4}$ $[m]$
Specific heat capacity C_p	2000 $[J/kgK]$	Outlet thickness h_2	$0.9144e^{-4}$ $[m]$
Thermal conductivity λ	0.14 $[W/mK]$	Slide length L	0.18288 $[m]$
Dynamic viscosity η_0	0.081 $[Pa.s]$	Ambient temperature Ta	20 $[°C]$
Lower wall operating speed U	31.946 $[m/s]$	Ambient pressure Pa	1 $[bar]$

The conservative form of the energy equation for the lubrication thin film flow of an incompressible fluid writes [1][1]:

$$\rho_0 C_p \left[\frac{\partial(uT)}{\partial x} + \frac{\partial(vT)}{\partial y}\right] = \lambda \frac{\partial^2 T}{\partial y^2} + \eta_0 \left(\frac{\partial u}{\partial y}\right)^2 \quad (1)$$

It contains the convection transport terms on its left hand side and the temperature diffusion and dissipation terms on its right hand side. The terms on the right hand side are simplified according to the lubrication thin film assumption, i.e. only derivatives across the thin film are taken into account.

The dimensionless coordinate $\bar{y}$ is introduced for taking into account that the film thickness h is not constant.

$$y = \bar{y} h(x) \quad (2)$$

Following this coordinate transformation, the energy equation (1) for the 1D slider becomes:

$$\rho_0 C_p \left[\frac{\partial(uT)}{\partial x} - \frac{\bar{y}}{h}\frac{\partial h}{\partial x}\frac{\partial(uT)}{\partial \bar{y}} + \frac{1}{h}\frac{\partial(vT)}{\partial \bar{y}}\right] = \lambda \frac{1}{h^2}\frac{\partial^2 T}{\partial \bar{y}^2} + \eta_0 \frac{1}{h^2}\left(\frac{\partial u}{\partial \bar{y}}\right)^2 \quad (3)$$

The slider is discretized with 2D computational cells as depicted in Error! Reference source not found.. Following the variable change described by (2), the computational domain is rectangular and orthogonal. The computational cell have four plane faces, denoted by lower-case letters corresponding to their direction (e, w, n, s) with respect to the central node P .

[1] Other forms of the energy equation are necessary for a compressible lubricant, for example using the (total) internal energy or the (total) enthalpy as a field variable.

Preprints (www.preprints.org) | NOT PEER-REVIEWED | Posted: 14 September 2018 doi:10.20944/preprints201809.0251.v1

Peer-reviewed version available at Lubricants 2018, 6, 95; doi:10.3390/lubricants6040095

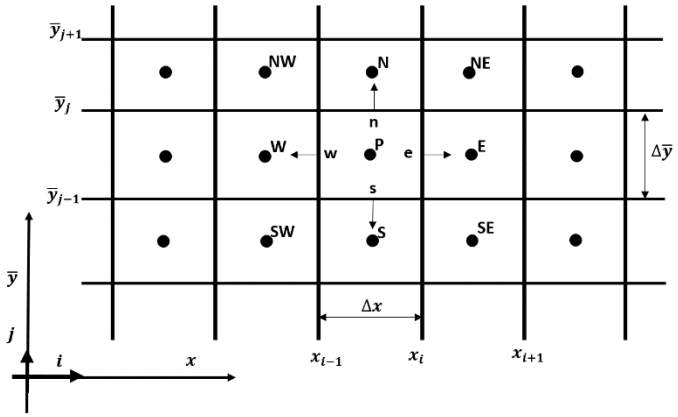

Figure 2. A typical 2D computational cell and the notation used for a 2D grid

In the natural discretization numerical approach, the energy equation is solved with the finite volume method [7]. Equation (3) is therefore integrated over the control volumes corresponding to the 2D computational cells:

$$\rho_0 C_p \int_{x_w}^{x_e}\int_{\bar{y}_s}^{\bar{y}_n}\left[\frac{\partial(uT)}{\partial x} - \frac{\bar{y}}{h}\frac{\partial h}{\partial x}\frac{\partial(uT)}{\partial \bar{y}} + \frac{1}{h}\frac{\partial(vT)}{\partial \bar{y}}\right]dxd\bar{y} = \lambda\frac{1}{h_P^2}\int_{x_w}^{x_e}\int_{\bar{y}_s}^{\bar{y}_n}\frac{\partial^2 T}{\partial \bar{y}^2}dxd\bar{y} + \eta_0\frac{1}{h_P^2}\left(\frac{\partial u}{\partial \bar{y}}\right)_P^2 \Delta x\Delta\bar{y} \tag{4}$$

Where the convection transport terms in x direction for example can be expressed:

$$\int_{x_w}^{x_e}\int_{\bar{y}_s}^{\bar{y}_n}\frac{\partial(uT)}{\partial x}dxd\bar{y} = [(uT)_e - (uT)_w]\Delta\bar{y} \tag{5}$$

An upwind discretization technique is used for the convective transport terms to avoid numerical instability [7]. For example at the east face of the control volume, the temperature T_e is up-winded based on the fluid flow direction. Mathematically, this can be express as:

$$(uT)_e = u_e\left[-T_P\frac{1-sgn(u_e)}{2} + T_E\frac{1-sgn(u_e)}{2} + T_P\right] \tag{6}$$

This yields the discretization form of equation (3):

$$(a_e + a_w + a_n + a_s)T_P - a_eT_E - a_wT_W - a_nT_N - a_sT_S - a_P(T_N - T_S) = \frac{\lambda}{\rho_0 C_p h_P^2}(T_N - 2T_P + T_S)\frac{\Delta x}{\Delta\bar{y}} + \frac{\eta_0}{\rho_0 C_p h_P^2}\left(\left.\frac{\partial u}{\partial y}\right|_P\right)^2 \Delta x\Delta\bar{y} \tag{7}$$

Where:

$$a_e = \frac{u_e[sgn(u_e)-1]}{2}\Delta\bar{y};\quad a_w = \frac{u_w[sgn(u_w)-1]}{2}\Delta\bar{y};$$

$$a_n = \frac{v_n[sgn(v_n)-1]}{2}\frac{\Delta x}{h_P};\quad a_s = \frac{v_s[sgn(v_s)-1]}{2}\frac{\Delta x}{h_P};\quad a_P = \frac{u_P\bar{y}_P}{2}\left.\frac{\partial h}{\partial x}\right|_P\frac{\Delta x}{h_P} \tag{8}$$

As stated in the introduction, the goal of the present work is to investigate the accuracy of the numerical solution of the energy equation given by the NDM and LPCM methods. Therefore, in order to avoid the uncertainties introduced by the numerical solution of the Reynolds equation, its analytic solution for the 1D slider is used.

Peer-reviewed version available at Lubricants 2018, 6, 95; doi:10.3390/lubricants6040095

Several other simplifying assumptions are needed for decoupling the Reynolds and the energy equation. Thus, the viscosity is considered constant and the flow regime laminar. Following the analytical solution, the pressure and the velocity in the 1D slider are [1]:

$$p(x) = \frac{6\eta_0 UL}{h_1 - h_2}\left(h^{-1} - \frac{h_1 h_2}{h_1 + h_2}h^{-2} - \frac{1}{h_1 + h_2}\right) \tag{9}$$

$$u(x,\bar{y}) = h^2 \frac{\bar{y}(\bar{y}-1)}{2\eta_0}\frac{\partial p}{\partial x} + (1-\bar{y})U \tag{10}$$

The velocity component across the thin film, v, is deduced by integrating the continuity equation (11) over the film thickness:

$$\frac{\partial u}{\partial x} + \frac{1}{h}\frac{\partial v}{\partial \bar{y}} - \frac{\bar{y}}{h}\frac{dh}{dx}\frac{\partial u}{\partial \bar{y}} = 0 \tag{11}$$

With the boundary conditions $v(x,\bar{y}=0) = 0$ and $v(x,\bar{y}=1) = 0$, this yields

$$v(x,\bar{y}) = -h\int_0^{\bar{y}} \frac{\partial u}{\partial x}\,d\bar{y} + \frac{dh}{dx}\int_0^{\bar{y}} \bar{y}\frac{\partial u}{\partial \bar{y}}\,d\bar{y} \tag{12}$$

It is to be underlined that in following approach only the BC at $\bar{y} = 0$ is used, while the second BC at $\bar{y} = 1$ is used to check the accuracy of the numerical integration.

The discretized system of equations given by (7) is solved using any numerical procedure for a linear system with a positive definite matrix. Grids with 80 equidistant cells in the x direction and different number of cells across the film thickness were used. The number of equidistant grid cells across the film thickness was Ny=10, 20, 40, 50, 80, 100, 160. In a first test, the ambient temperature 20°C was imposed on the lower and upper walls, so as the inlet and outlet temperatures. The dimensionless wall temperature gradient was monitored[2]. This dimensionless wall temperature gradient is defined by:

$$\frac{d\bar{T}(x,\bar{y})}{d\bar{y}} = \frac{1}{T_a}\frac{dT(x,\bar{y})}{d\bar{y}} \tag{13}$$

Where $T_a = T_{inlet} - 273K$ is a reference temperature.

The results are depicted in **Figure 3** and **Figure 4** and show that the curves become superposed starting with Ny=80 cells. An estimation of the accuracy is obtained by using the relative error of the wall temperature gradients which is defined in (14).

$$\varepsilon = \frac{\sqrt{\frac{1}{n}\sum_{i=1}^{n}\left(\frac{d\bar{T}_{N_y}(x_i,\bar{y})}{d\bar{y}} - \frac{d\bar{T}_{ref}(x_i,\bar{y})}{d\bar{y}}\right)^2}}{\sqrt{\frac{1}{n}\sum_{i=1}^{n}\left(\frac{d\bar{T}_{ref}(x_i,\bar{y})}{d\bar{y}}\right)^2}} \quad for\ \bar{y}=0\ or\ \bar{y}=1 \tag{14}$$

Where the $\bar{T}_{ref}$ obtained with the finest grid Ny=160 is considered as the reference solution.

The variation of these errors with the number of grid cells across the film thickness is depicted in **Figure 5(a).** For Ny=80 the dimensionless error is less than 3% and the accuracy of the numerical solution is acceptable.

The computational time is depicted in **Figure 5(b).** A rapid increase of the computational time with the grid cells must be underlined. For example, the calculation case with Ny=80 grid cells requires 1,844s while the computational time of the case with Ny=160 cells is one order of magnitude higher.

[2] This is equivalent to monitoring the wall heat fluxes.

Preprints (www.preprints.org) | NOT PEER-REVIEWED | Posted: 14 September 2018 doi:10.20944/preprints201809.0251.v1

Peer-reviewed version available at Lubricants 2018, 6, 95; doi:10.3390/lubricants6040095

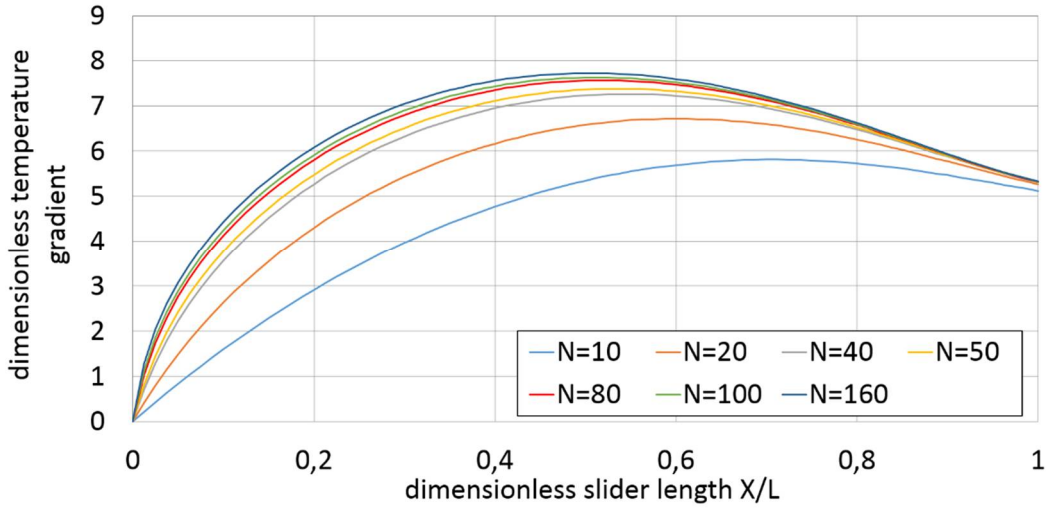

Figure 3. Dimensionless temperature gradient at the lower wall for NDM solution and imposed wall temperatures (**h1/h2=2**, Nx=80 cells)

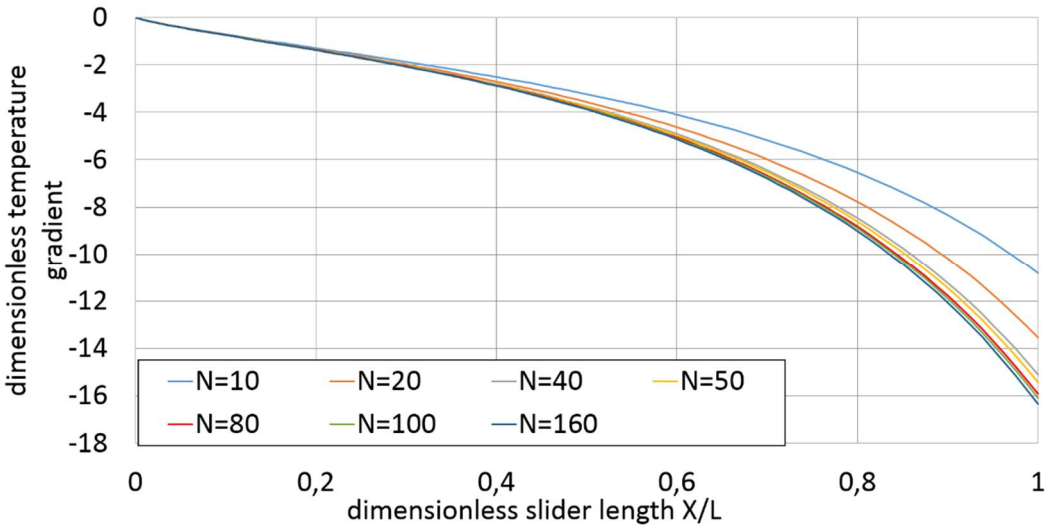

Figure 4. Dimensionless temperature gradient at the upper wall for NDM solution and imposed wall temperatures (**h1/h2=2**, Nx=80 cells)

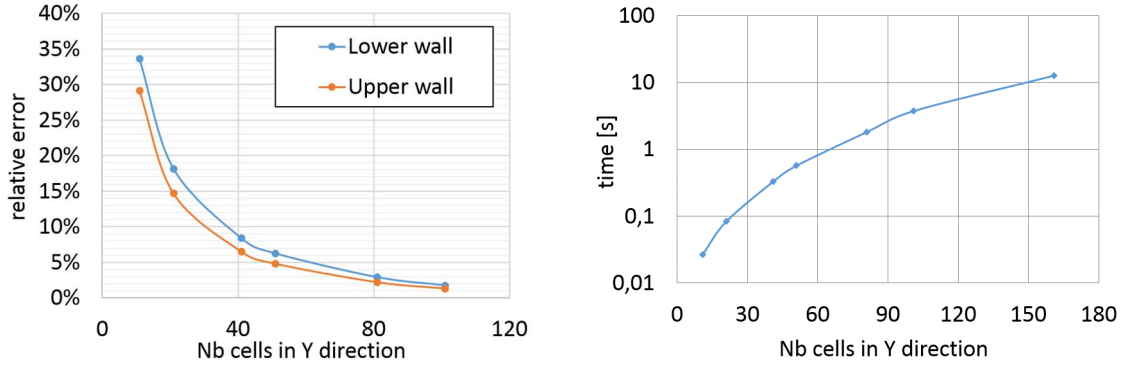

(**a**) (**b**)

Figure 5. (a) Relative error and (b) computational time of NDM solution for Y direction grid refinements (**h1/h2=2**, Nx=80 cells)

Preprints (www.preprints.org) | NOT PEER-REVIEWED | Posted: 14 September 2018 doi:10.20944/preprints201809.0251.v1

Peer-reviewed version available at Lubricants 2018, 6, 95; doi:10.3390/lubricants6040095

3. The numerical solution of the energy equation based on the Lobatto points collocation method

The Lobatto Point Collocation Method (LPCM) is based on the approximation of the temperature with Legendre polynomials across the film thickness. Because Legendre polynomials are defined on the interval $[-1, 1]$, the following coordinate transformation is used:

$$y = \frac{(\zeta + 1)h}{2} \tag{15}$$

Where ζ is the new dimensionless coordinate across the film thickness.

Following the coordinate transformation, the energy equation (1) becomes:

$$\rho C_p \left[\frac{\partial(uT)}{\partial x} - \frac{(\zeta+1)}{h}\frac{\partial h}{\partial x}\frac{\partial(uT)}{\partial \zeta} + \frac{2}{h}\frac{\partial(vT)}{\partial \zeta}\right] = \lambda \frac{4}{h^2}\frac{\partial^2 T}{\partial \zeta^2} + \eta_0 \frac{4}{h^2}\left(\frac{\partial u}{\partial \zeta}\right)^2 \tag{16}$$

For an incompressible lubricant with constant viscosity, only the variable temperature T is approximated across the film thickness.

$$T(x, \zeta) = \sum_{j=0}^{N} \hat{T}_j(x) P_j(\zeta) \tag{17}$$

Where N is the highest order of the Legendre polynomials, $P_j(\zeta)$ its jth order and $\hat{T}_j(x)$ its jth coefficient.

This description holds for every point in the 2D computational domain. Compared to the NDM which computes directly the temperature by solving the energy equation discretized over the film thickness, the LPCM calculates the polynomial coefficients of temperature $\hat{T}_j$. The coefficients of the Legendre polynomials expansion can be obtained using different methods but it is accepted that the most reliable is the collocation method using the Lobatto points. The Lobatto points are the roots of the derivative of the highest degree of the Legendre polynomial (i.e. the roots of $dP_N/d\zeta$).

For a given position in the x direction, the temperature is replaced by its approximation (17) across the fluid film and the energy equation (16) is enforced to hold true for each Lobatto point, $\zeta_j, j \in [1, \ldots, N-1]$. This leads to N-1 partial differential equations with the unknown $\hat{T}_j$. The boundary conditions are applied at the two walls, $\zeta = -1$ and $\zeta = 1$, which leads the other two equations. In total, a system of N+1 equations for the N+1 unknown $\hat{T}_j$ is obtained.

Figure 6 and **Figure 7** depict the dimensionless wall temperature gradient obtained with an increasing order of the Legendre polynomials.

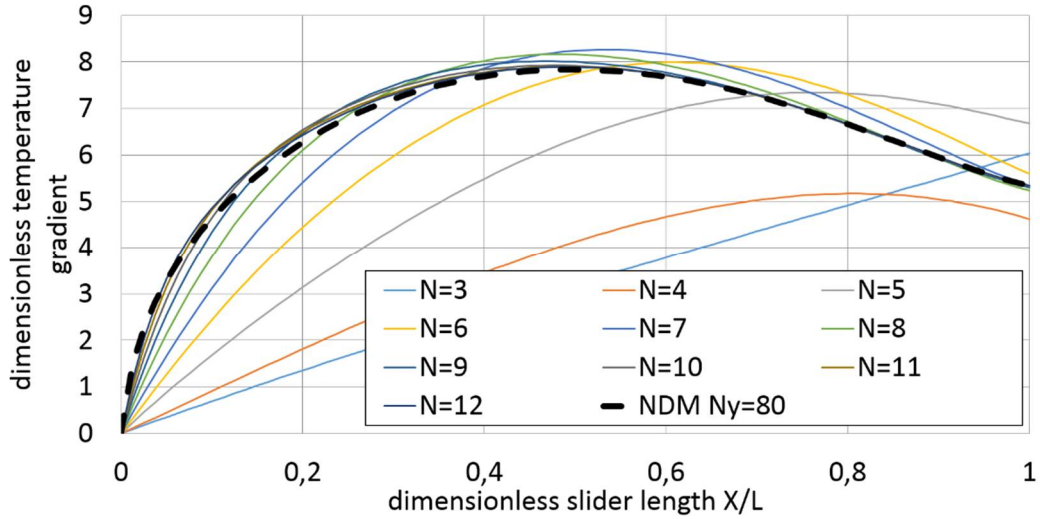

Figure 6. Dimensionless temperature gradient at the lower wall for LPCM solution and imposed wall temperatures (**h1/h2=2**, Nx=80 cells)

Preprints (www.preprints.org) | NOT PEER-REVIEWED | Posted: 14 September 2018 doi:10.20944/preprints201809.0251.v1

Peer-reviewed version available at Lubricants 2018, 6, 95; doi:10.3390/lubricants6040095

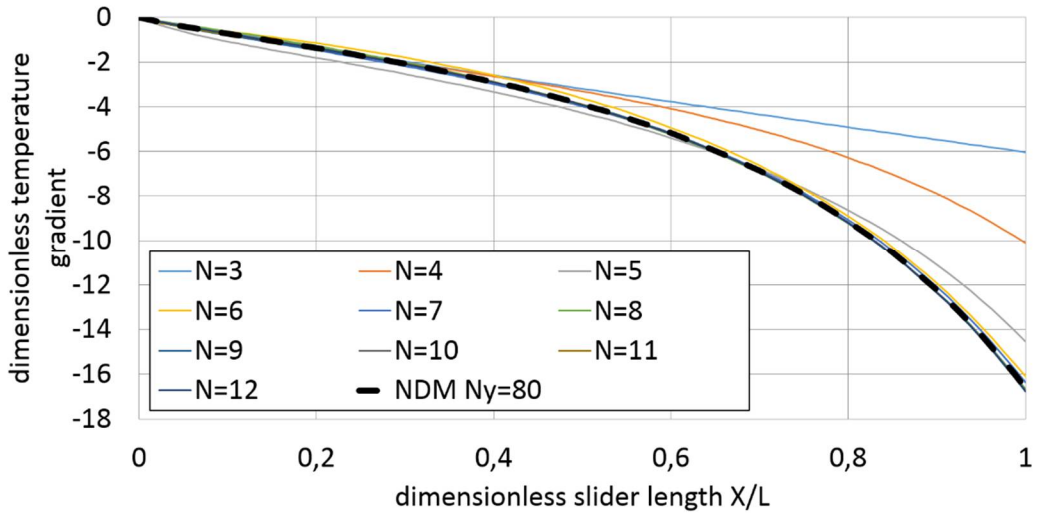

Figure 7. Dimensionless temperature gradient at the upper wall for LPCM solution and imposed wall temperatures (**h1/h2=2**, Nx=80 cells)

The reference results used for comparison are given by the NDM with Ny=80 grid cells. The relative error between the reference results and the wall temperature gradient obtained with the LPCM is defined as:

$$\varepsilon = \frac{\sqrt{\frac{1}{n}\sum_{i=1}^{n}\left(\frac{2\partial \bar{T}_{N_{Lobbato}}(x_i,\zeta)}{\partial \zeta} - \frac{\partial \bar{T}_{ref_{NDM}}(x_i,\bar{y})}{d\bar{y}}\right)^2}}{\sqrt{\frac{1}{n}\sum_{i=1}^{n}\left(\frac{d\bar{T}_{ref_{NDM}}(x_i,\bar{y})}{d\bar{y}}\right)^2}} \quad (18)$$

Where $\zeta = 1$ or $\zeta = -1$ for LPCM and $\bar{y} = 1$ or $\bar{y} = 0$ for NDM.

The relative errors are depicted in **Figure 8(a)** and show that the approximation of the temperature variation with Legendre polynomials of degree 8 yields grid independent solution. It is to be remarked that a non-negligible difference holds for the temperature gradient at the lower wall (**Figure 6**) where the error converges toward 6%. This is due the uncertainties of the reference results obtained with the NDM solution and Ny=80 that are used for comparisons. If comparing the results of the LPCM solution with the NDM solution and Ny=160, the lower wall relative error decreases to 2%. This shows the high accuracy of the LPCM solution with Legendre polynomials of degree no larger than 8.

The computational effort is depicted in **Figure 8(b)**. Again, the reference NDM results are obtained with Ny=80. Compared with the reference solution, the computational time of the LPCM solution is divided by four or three because only a limited expansion of Legendre polynomials is sufficient to obtain grid independent results.

For comparison, the temperature fields obtained with LPCM ($N_{Lobatto}$=10) and NDM (Ny=80) are depicted in Figure A1 and A2 of the Appendix.

Preprints (www.preprints.org) | NOT PEER-REVIEWED | Posted: 14 September 2018 doi:10.20944/preprints201809.0251.v1

Peer-reviewed version available at Lubricants 2018, 6, 95; doi:10.3390/lubricants6040095

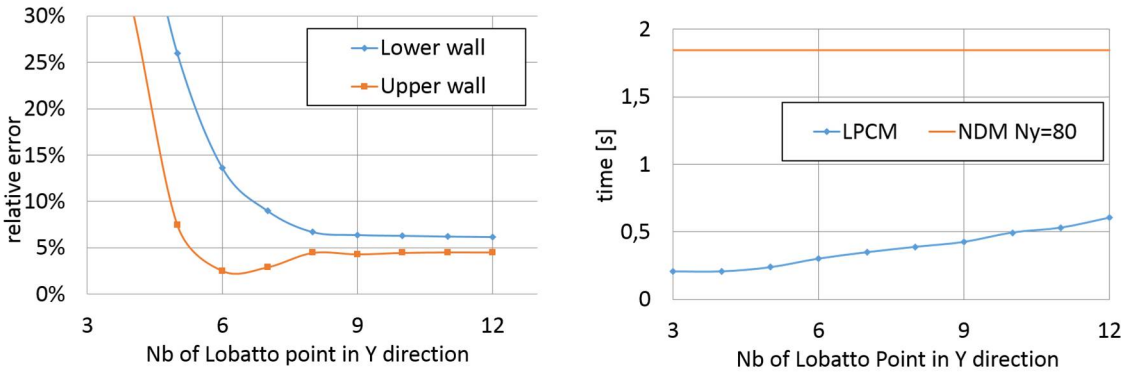

198 **Figure 8.** Relative error (a) and computational time (b) of the LPCM solution for Y direction grid
199 refinements (**h1/h2=2**, Nx=80 cells)

200 **4. Further comparison of numerical results obtained by NDM and LPCM**

201 The previous results were obtained for a linear converging 1D slider with inlet/outlet film
202 thickness ratio h1/h2=2, imposed wall temperatures (Dirichlet BC) and completely decoupled from
203 Reynolds equation. Other simple cases of the converging 1D slider are also investigated and bring
204 interesting conclusions.

205 *4.1. Different geometrical configurations of 1D slider*

206 Two other inlet/outlet film thickness ratios, h1/h2=4 and h1/h2=8 were investigated, while
207 keeping the same wall temperature boundary conditions and the decoupled Reynolds equation. The
208 increased inlet/outlet film thickness ratio lead to a slower convergence of the NDM results with the
209 Y grid refinements, therefore the solution obtained with Ny=160 was considered as the reference
210 results. The number of computational cells in x direction was kept the same (Nx=80 cells).
211 The results obtained for h1/h2=4 are depicted from **Figure 9** to **Figure 11**.
212

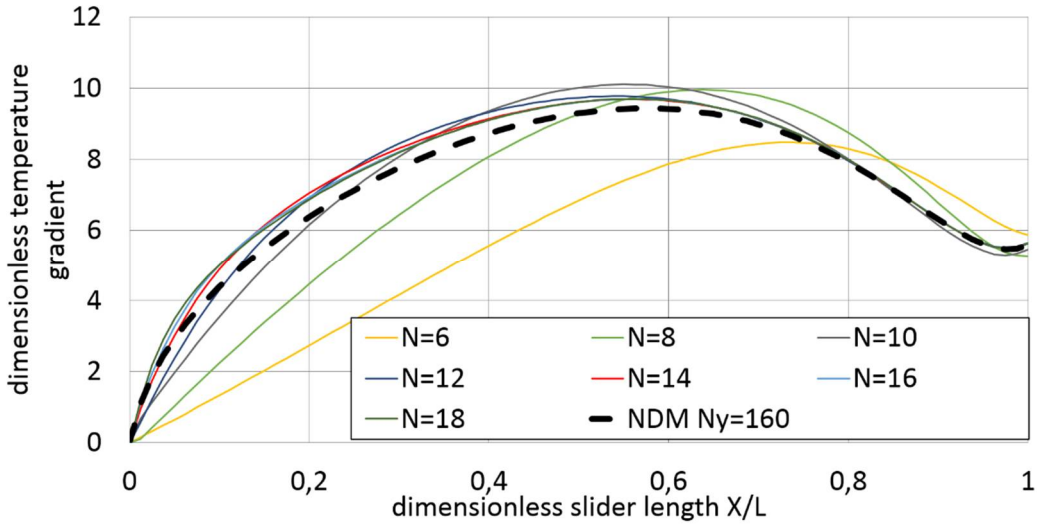

213 **Figure 9.** Dimensionless temperature gradient at the lower wall for LPCM solution and imposed
214 wall temperatures (**h1/h2=4**, Nx=80 cells)

Preprints (www.preprints.org) | NOT PEER-REVIEWED | Posted: 14 September 2018 doi:10.20944/preprints201809.0251.v1

Peer-reviewed version available at Lubricants 2018, 6, 95; doi:10.3390/lubricants6040095

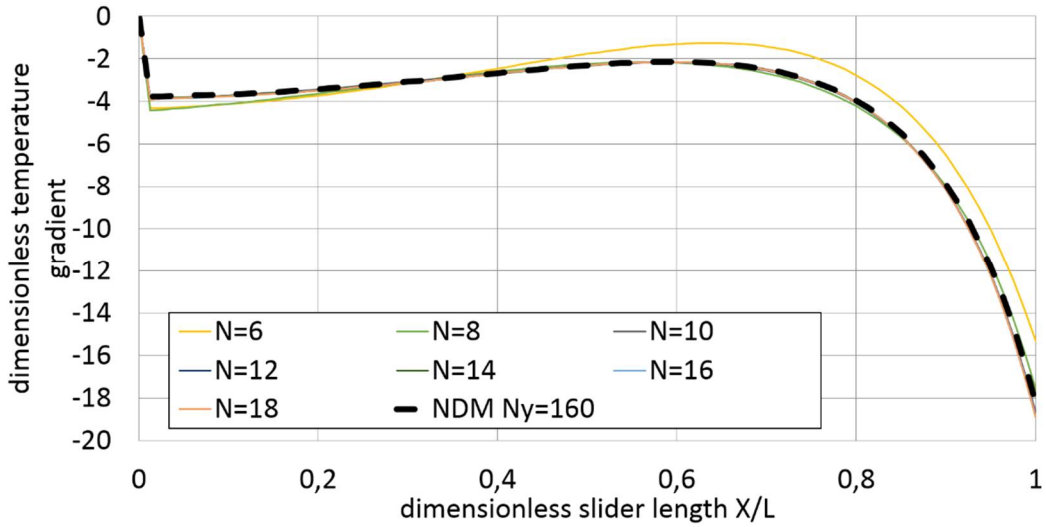

Figure 10. Dimensionless temperature gradient at the upper wall for LPCM solution and imposed wall temperatures (**h1/h2=4**, Nx=80 cells)

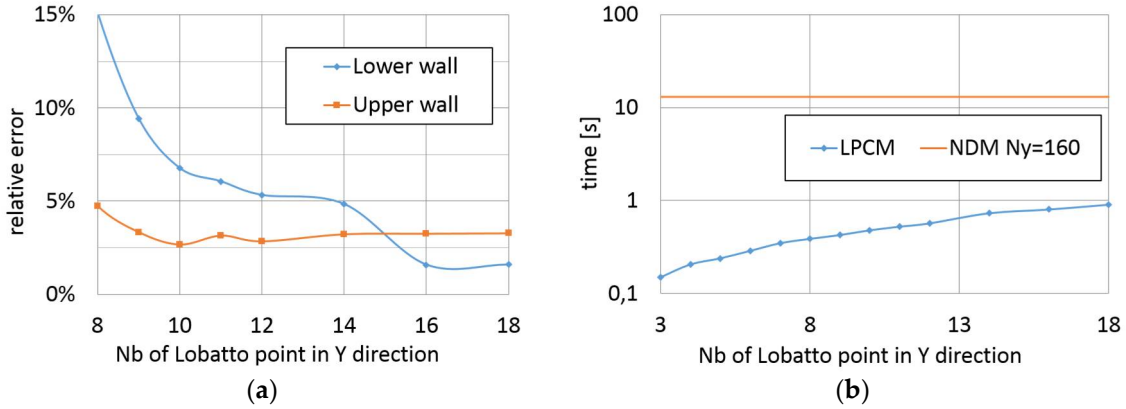

Figure 11. Relative error (a) and computational time (b) of LPCM solution for Y direction grid refinements (**h1/h2=4**, Nx=80 cells)

The lower and upper wall results show different trends. The upper wall temperature gradient reaches grid convergence starting with N=10 Legendre polynomials while the resolution of the lower wall gradient needs N=16 Legendre polynomials. However, **Figure 11(b)** shows that even when using a high number of Legendre polynomials, the LPCM requires one order of magnitude less computational time than the NDM of the same accuracy.

The results obtained for h1/h2=8 are depicted from **Figure 12** to **Figure 14**. The same remarks as for h1/h2=4 can be drawn except for the fact that this time both the upper and the lower wall temperature reach grid convergence only with N=16 Legendre polynomials. **Figure 14(b)** shows that the computational time of the NDM with Ny=160 increases for this calculation case. It can be seen from **Figure 11(b)** and **Figure 14(b)** that the computational effort of the NDM increases one order of magnitude with increasing the ratio h1/h2 from 4 to 8. This is not the case for the LPCM that requires the same computational time for these two cases, one or two order of magnitude lower than the LPCM. LPCM remains therefore largely superior to NDM in terms of computational time.

The temperature fields obtained with LPCM ($N_{Lobatto}$=10) and NDM (Ny=160) are depicted in Figure A3-A6 of the Appendix.

Preprints (www.preprints.org) | NOT PEER-REVIEWED | Posted: 14 September 2018 doi:10.20944/preprints201809.0251.v1

Peer-reviewed version available at Lubricants 2018, 6, 95; doi:10.3390/lubricants6040095

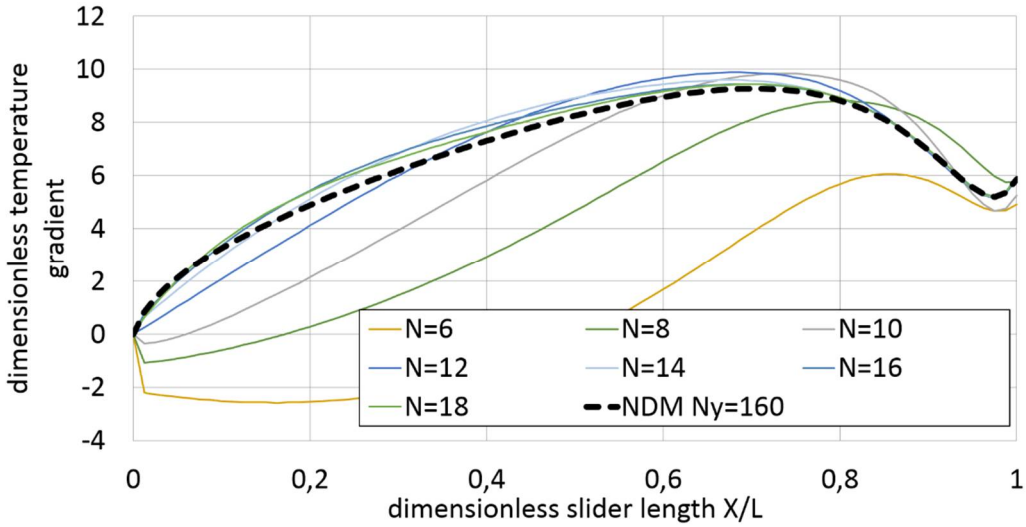

Figure 12. Dimensionless temperature gradient at the lower wall for LPCM solution and imposed wall temperatures (**h1/h2=8**, Nx=80 cells)

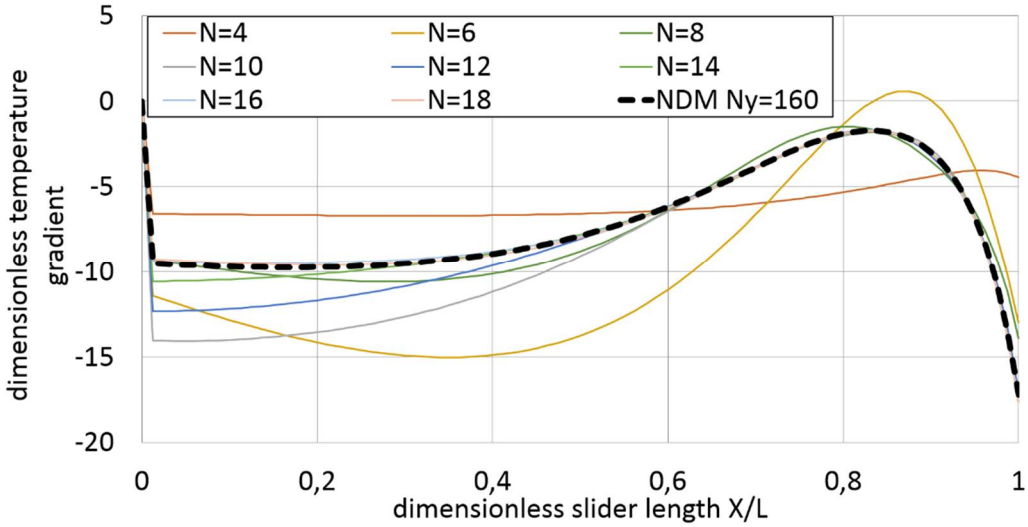

Figure 13. Dimensionless temperature gradient at the upper wall for LPCM solution and imposed wall temperatures (**h1/h2=8**, Nx=80 cells)

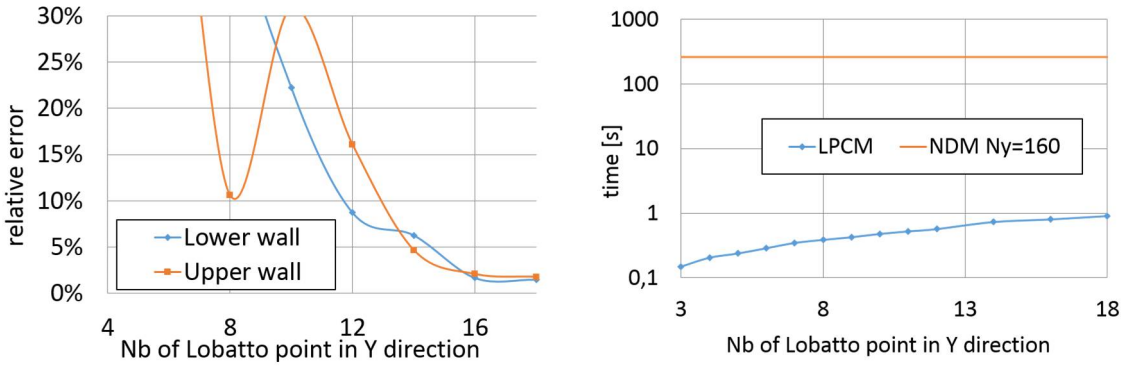

Figure 14. Relative error (a) and computational time (b) of LPCM solution for Y direction grid refinements (**h1/h2=8**, Nx=80 cells)

Preprints (www.preprints.org) | NOT PEER-REVIEWED | Posted: 14 September 2018 doi:10.20944/preprints201809.0251.v1

Peer-reviewed version available at Lubricants 2018, 6, 95; doi:10.3390/lubricants6040095

4.2. Different thermal boundary conditions applied to 1D slider

The previous cases dealt with imposed wall temperatures while the wall temperature gradient was a calculation result. In the following test, the lower wall of the 1D slider is adiabatic, i.e. $(\partial T/\partial y)_{LowerW} = 0$ while the temperature of the upper wall is $T_{UpperW} = 30°C$. The film thickness ratio is h1/h2=4 and the inlet temperature $T_{inlet} = 20°C$. For the LPCM, 10 Lobatto points are used and the results are compared to the NDM (Nx=80 cells and Ny=160 cells all equidistant). **Figure 15** and **Figure 16** show the perfect resolution of the upper wall temperature gradient and of the lower wall temperature.

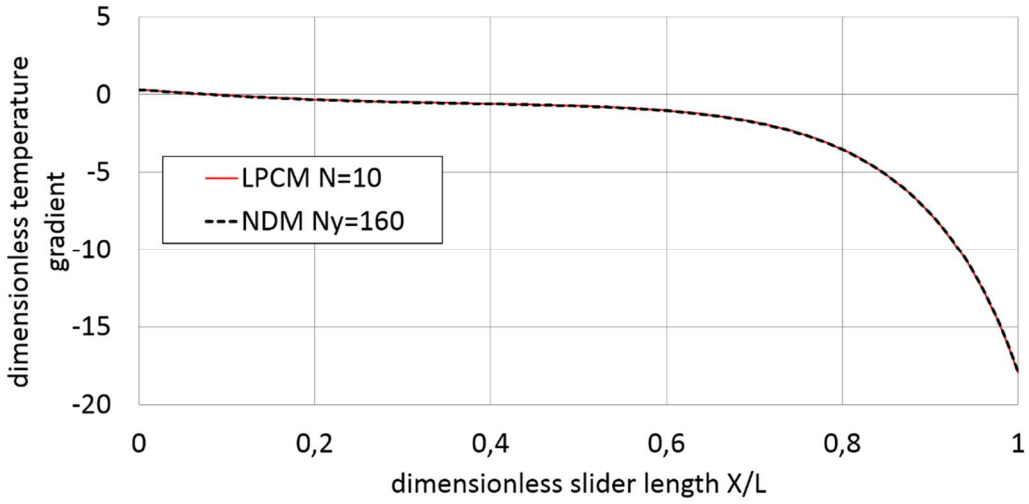

Figure 15. Dimensionless temperature gradient at the upper wall
$(\mathbf{T_{UpperW} = 30°C},\ \mathbf{(\partial T/\partial y)_{LowerW} = 0}, \boldsymbol{T_{inlet} = 20°C}; \boldsymbol{T_{outlet} = 20°C})$

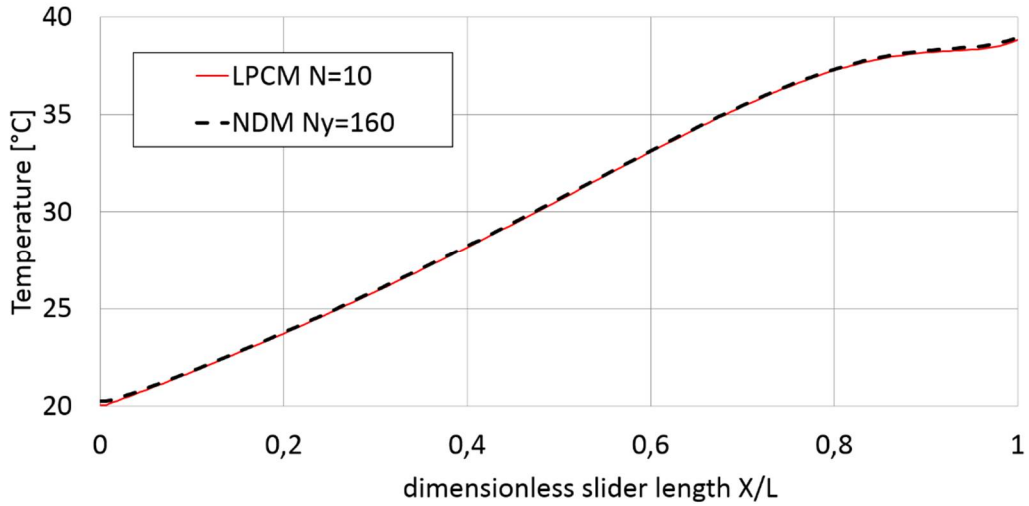

Figure 16. Temperature at the lower wall
$(\mathbf{T_{UpperW} = 30°C},\ \mathbf{(\partial T/\partial y)_{LowerW} = 0}, \boldsymbol{T_{inlet} = 20°C}; \boldsymbol{T_{outlet} = 20°C})$

A different test case consists of imposing different wall temperatures, $T_{UpperW} = 30°C$, $T_{LowerW} = 20°C$ and $T_{inlet} = 20°C$. The LPCM is performed with 10 and 14 Lobatto points and the previous resolution was used for the NDM. Results are depicted in **Figure 17** and **Figure 18** and show that for the lower wall errors subsist close to the inlet section. The errors remain present with increasing the number of Lobatto points.

The temperature fields of these two last cases are depicted in Figure A7-A10 of the Appendix.

Preprints (www.preprints.org) | NOT PEER-REVIEWED | Posted: 14 September 2018 doi:10.20944/preprints201809.0251.v1

Peer-reviewed version available at Lubricants 2018, 6, 95; doi:10.3390/lubricants6040095

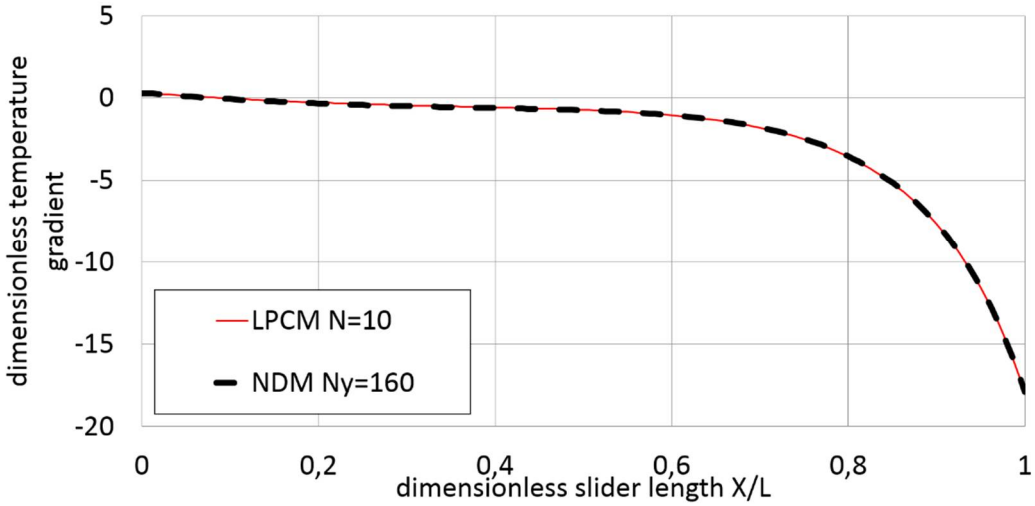

Figure 17. Dimensionless temperature gradient at the upper wall ($\mathbf{T_{UpperW} = 30°C}$, $\mathbf{T_{LowerW} = 20°C}$, $\boldsymbol{T_{inlet} = 20°C}$; $\boldsymbol{T_{outlet} = 20°C}$)

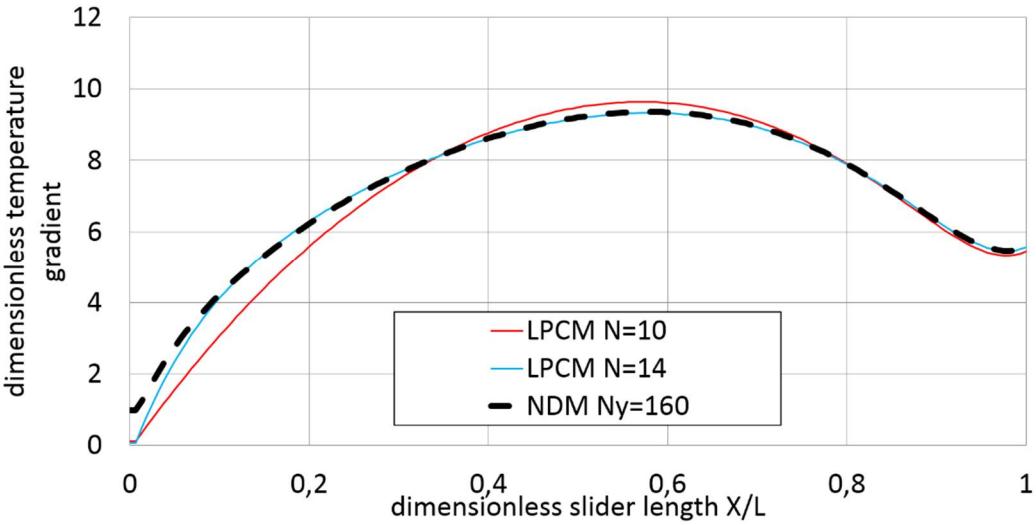

Figure 18. Dimensionless temperature gradient at the lower wall ($\mathbf{T_{UpperW} = 30°C}$, $\mathbf{T_{LowerW} = 20°C}$, $\boldsymbol{T_{inlet} = 20°C}$; $\boldsymbol{T_{outlet} = 20°C}$)

5. Results for the energy equation coupled with Reynolds equation

The above presented results showed the grid refinements required for obtaining accurate solutions of the energy equation when decoupled from the Reynolds equation. The viscosity of a liquid lubricant depends strongly on the temperature and therefore decoupling is not possible[3]. For this reason, data found in the literature deal directly with the complete thermo-hydrodynamic analysis of the 1D slider [3] presented previously.

This thermo-hydrodynamic (THD) coupled analysis is subsequently performed for the 1D slider case. The results of the LPCM are compared with the data from [3]. Their grid convergence and the computational time are analyzed by comparisons with NDM results. This step completes the validation of the decoupled energy equation described in the previous paragraphs.

A temperature dependent viscosity following an exponentially decaying law $\eta(T) = 0.13885e^{-0.045(T-T_{ambient})}$ is used to replace the constant viscosity η_0. The rest of the geometrical and physical parameters are the same as in the previous case. The inlet and wall temperatures are equal to the ambient reference temperature. As for the variations of the temperature across the thin film,

[3] The same is not true for aerodynamic bearings operating with very thin air films.

Peer-reviewed version available at Lubricants 2018, 6, 95; doi:10.3390/lubricants6040095

the terms in the generalized Reynolds equation with variable viscosity are also discretized by Legendre polynomials and the coefficients are obtained by collocation at the Lobatto points.

The computational domain of the 1D slider is discretized using Nx=30 equidistant cells in the main flow direction and 10 Lobatto points across the film thickness. The Reynolds and the energy equations are numerically solved following a segregated approach.

Figure 19(a) compares the pressure variation in the 1D slider obtained with the LPCM and the one given in [3]. **Figure 19(b)** presents the variation of the outlet temperature difference across the film thickness. Both the pressure and the temperature variations obtained with the LPCM are in agreement with [3].

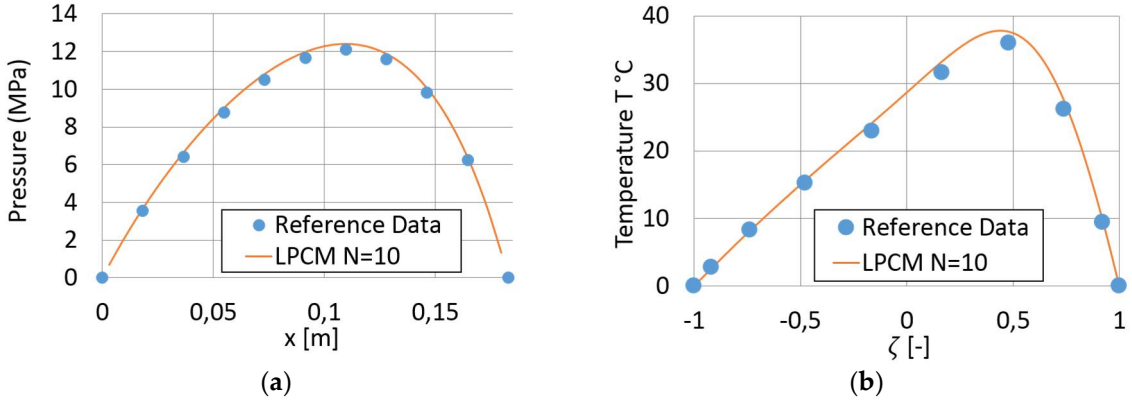

Figure 19. (a) Pressure variation in the 1D slider (h1/h2=2), coupled THD solution and (b) Outlet temperature variation across the film thickness in the 1D slider (h1/h2=2), coupled THD solution

This 1D non-isothermal slider is also used to compare the efficiency of the LPCM with the NDM. Several calculations are performed with the NDM method in order to check the grid convergence and for obtaining results that could serve as a reference. These tests use seven grid refined in the Y direction (Ny=10, 20, 40, 60, 80, 100, and 120 equally spaced control volumes) while a constant number of 30 control volumes is used in the x direction. The relative error ε_K in terms of wall temperature gradients between two successive grids is defined as:

$$\varepsilon_K = \frac{\sqrt{\frac{1}{n}\sum_{i=1}^{n}\left(\frac{\partial T_K(y)}{\partial y} - \frac{\partial T_{K+1}(y)}{\partial y}\right)^2}}{\sqrt{\frac{1}{n}\sum_{i=1}^{n}\left(\frac{\partial T_{K+1}(y)}{\partial y}\right)^2}} \tag{19}$$

Where the subscript K indicates the grid refinement level in the y direction.

Figure 20(a) shows that a minimum number of 40 cells in y direction is necessary to reach a satisfactory grid-independent solution. The computational time is depicted in **Figure 20(b)**. Thus, the solution obtained by NDM with 40 equally spaced cells over the film thickness is considered as the reference for the 1D thermo-hydrodynamic slider test case.

Preprints (www.preprints.org) | NOT PEER-REVIEWED | Posted: 14 September 2018 doi:10.20944/preprints201809.0251.v1

Peer-reviewed version available at Lubricants 2018, 6, 95; doi:10.3390/lubricants6040095

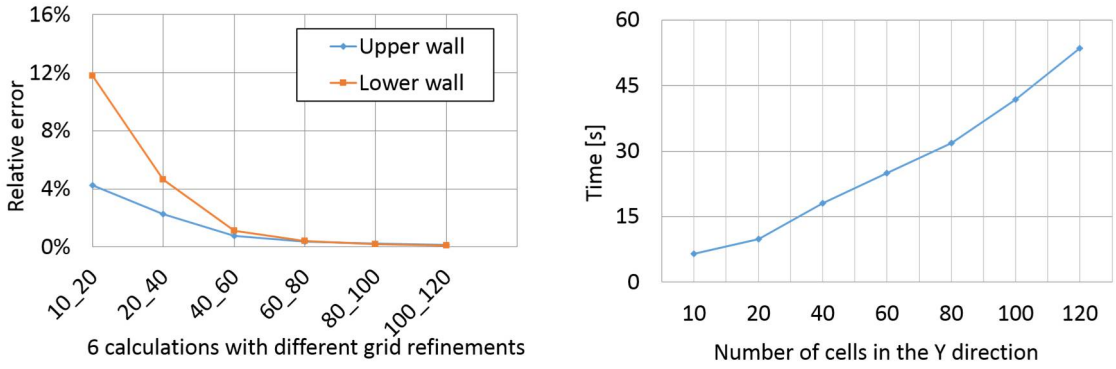

(a) (b)

Figure 20. (a) Relative error ε_K of the NDM method for different grid refinements and (b) Computational time of NDM for different numbers of cells over the film thickness for the 1D THD slider

The LPCM results obtained with different numbers of Lobatto points are compared with the reference NDM solution. In **Figure 21(a)**, the relative error drops rapidly and remains below 2% starting with 11 Lobatto points. **Figure 21(b)** shows that the computational time for the LPCM does not exceed 2 seconds while the reference method takes about 18 seconds.

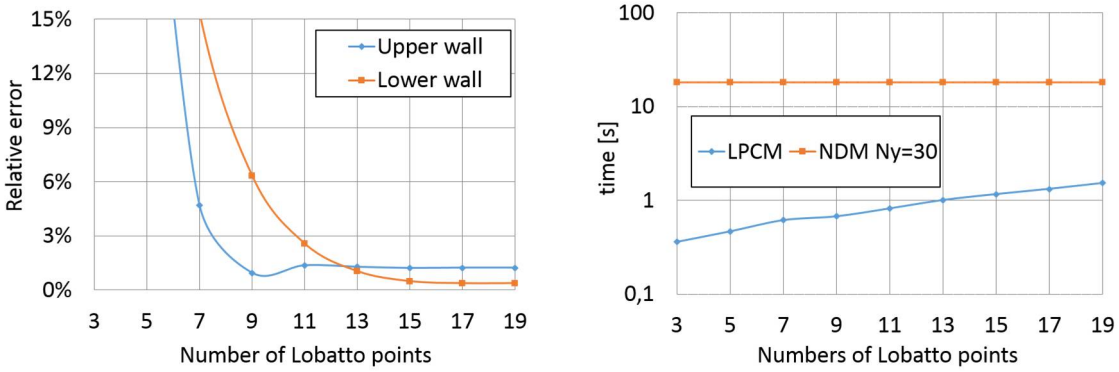

(a) (b)

Figure 21. (a) Relative error ε_N between LPCM and the reference NDM Ny=30 and (b) Computational time of LPCM compared to the reference NDM Ny=30 results for the 1D THD slider.

6. Example of a two-lobe journal bearing

The coupled Reynolds and energy equations represent a solver for thermo-hydrodynamic problems in lubricated journal and thrust bearings. However, pure validations are more difficult in the context of lubricated bearings because of the additional effects such as the film rupture and reformation (cavitation) that must be modeled and dealt with ([9], [10], [11]).

Not the least, several user-defined heat transfer parameters must be specified and this is mainly done in a trial and error approach. The uncertainties in this kind of problems may therefore be quite important and comparisons with experimental data are not exactly validations of the numerical approaches.

For the completeness of the present work, the numerical analysis of a real journal bearing is presented in the following. The recent experimental results published by Giraudeau et al. [8] in 2016 for a two-lobe journal bearing with axial supply grooves are used for comparing numerical predictions with experimental results. The length of the tested bearing is 68.4 mm and its diameter is 100 mm. The radial assembly clearance is 68 μm while the radial bearing clearance is 143 μm. The bearing is lubricated by an ISO VG 46 oil supplied at a constant pressure of 0.17 MPa and a temperature of 43°C. The following oil characteristics are used for the calculations: $\rho = 850\ kg/m^3$,

Preprints (www.preprints.org) | NOT PEER-REVIEWED | Posted: 14 September 2018 doi:10.20944/preprints201809.0251.v1

Peer-reviewed version available at Lubricants 2018, 6, 95; doi:10.3390/lubricants6040095

$C_p = 2000\,J/(kgK)$ and $\lambda = 0.13\,W/(mK)$. The viscosity of the oil is $0.0416\,Pa.s$ at $40°C$ and $0.0191\,Pa.s$ at $60°C$. The variation is described by an exponentially decaying law.

Only the results for the lower, loaded lobe are shown here. Cavitation was dealt with by using the algorithm introduced in [11]. This algorithm uses a free boundary formulation of the incompressible Reynolds equation. The problem is then solved with an efficient solver based on Fischer-Burmeister form, Newton algorithm and Shur's complement.

The shaft is considered to have a constant temperature estimated from experiments while adiabatic wall conditions are imposed on the bushing. The computational domain is discretized using 32×16 cells in circumferential and axial directions while 11 Lobatto points are used to describe the temperature variation across the fluid film.

Figure 22(a) and **Figure 22(b)** depict the pressure and the temperature variations in the circumferential direction of the bearing mid plane. The predicted pressures show good agreement with the measurements. The predicted temperature shows a reasonable agreement with the measurements and the quality of the prediction could be improved by including the thermal deformation of the bushing and by refining the boundary conditions for the energy equation.

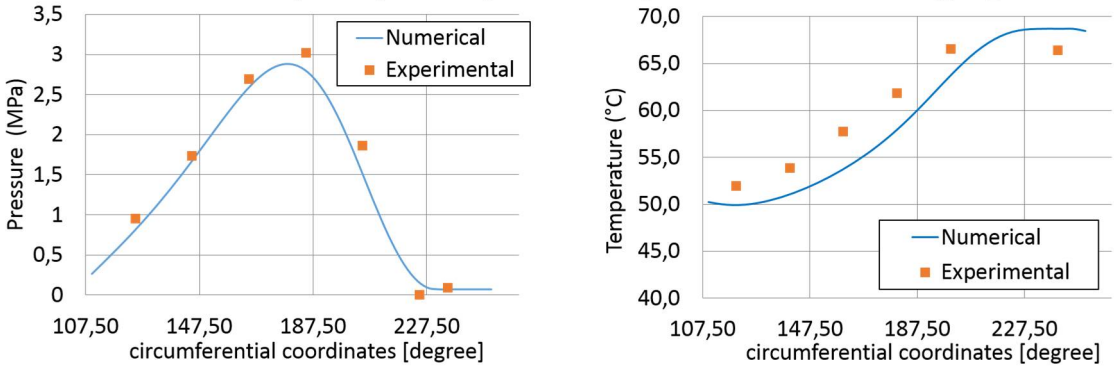

Figure 22. (a) Comparison of measured pressures and current numerical results in the mid plane of the loaded lobe (3500 rpm, 6kN load) and (b) Comparisons of measured temperatures and current numerical results in the mid plane of the loaded lobe (3500 rpm, 6kN load)

7. Conclusions

The present work is focused on the numerical solution of the energy equation in very simple test cases as part of thin fluid films lubrication. The work was motivated by the fact that the complete energy equation has no analytic solution that can be used for comparisons in validations. Therefore, an energy equation decoupled from Reynolds equation in the case of the 1D slider was imagined for which the analytical solution of the velocity field was used. The second concern was an efficient solver for the energy equation. Two numerical methods were compared, the NDM based on a finite volume discretization and the LPCM based on a Legendre polynomial approximation of the temperature across the film thickness. The LPCM proved to be one or two orders of magnitudes more efficient than the NDM in terms of computation time. This is not negligible if one takes into account that when coupled, the Reynolds and the energy equations are numerically solved in segregated and iterative manner. The thermo-hydrodynamic calculation of a 1D slider (i.e. for coupled Reynolds and energy equation) confirm this conclusion.

Comparisons of the LPCM thermo-hydrodynamic analyses with the experimental results obtained in a two lobes journal bearing are also presented. However, they are not considered as real validations of the numerical model since very simple and intuitive boundary conditions of the energy equation were used. Alternatively, the results presented for the 1D slider may be used for validating the first development steps of any solver based on the energy equation for thin film flows.

Preprints (www.preprints.org) | NOT PEER-REVIEWED | Posted: 14 September 2018 doi:10.20944/preprints201809.0251.v1

Peer-reviewed version available at Lubricants 2018, 6, 95; doi:10.3390/lubricants6040095

Appendix: Temperature fields

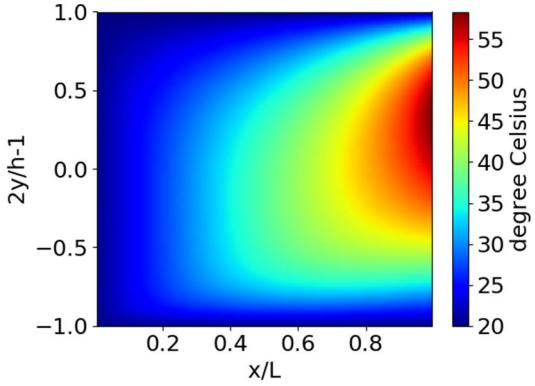

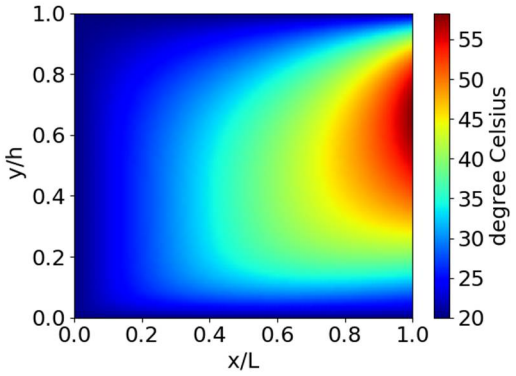

$h1/h2 = 2, \quad T_{UpperW} = 20°C, \quad T_{LowerW} = 20°, \quad T_{inlet} = 20°C, \quad T_{outlet} = 20°C$

Figure A1: LPCM, $N_{Lobatto}$=10

Figure A2: NDM, N_y=80

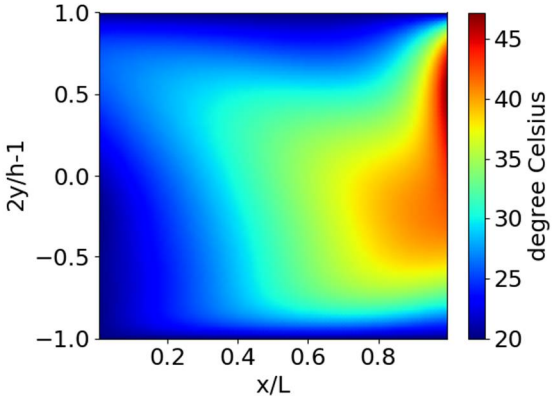

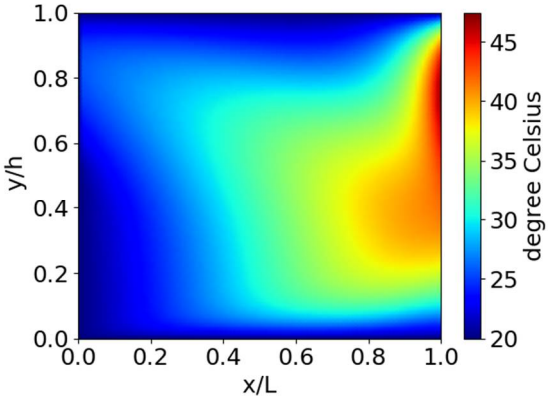

$h1/h2 = 4, \quad T_{UpperW} = 20°C, \quad T_{LowerW} = 20°, \quad T_{inlet} = 20°C, \quad T_{outlet} = 20°C$

Figure A3: LPCM, $N_{Lobatto}$=10

Figure A4: NDM, N_y=160

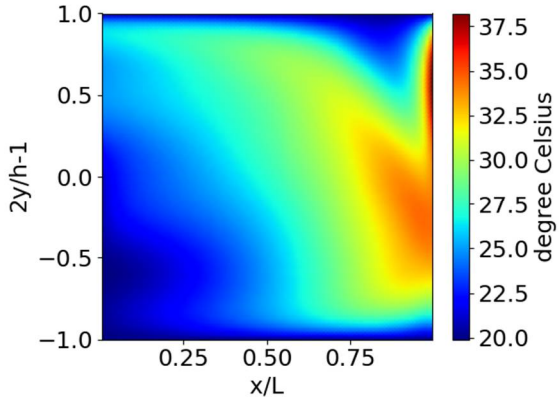

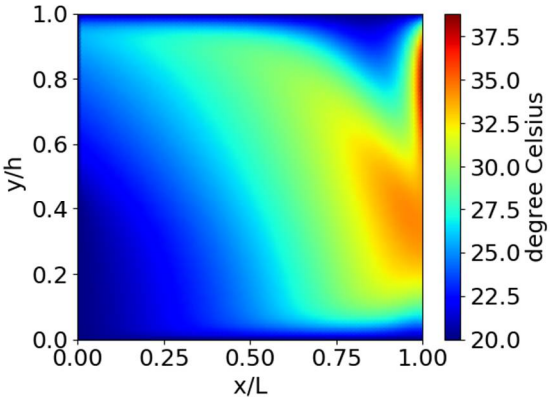

$h1/h2 = 8, \quad T_{UpperW} = 20°C, \quad T_{LowerW} = 20°, \quad T_{inlet} = 20°C, \quad T_{outlet} = 20°C$

Figure A5: LPCM, $N_{Lobatto}$=10

Figure A6: NDM, N_y=160

Preprints (www.preprints.org) | NOT PEER-REVIEWED | Posted: 14 September 2018 doi:10.20944/preprints201809.0251.v1

Peer-reviewed version available at Lubricants 2018, 6, 95; doi:10.3390/lubricants6040095

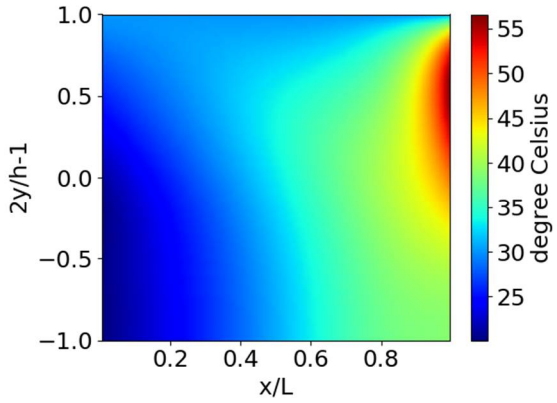

Figure A7: LPCM, $N_{Lobatto}$=10

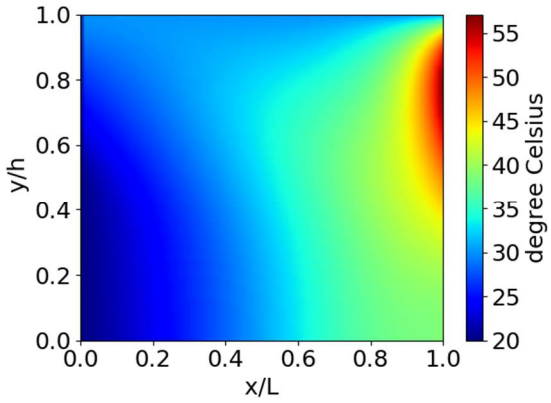

Figure A8: NDM, N_y=160

$h1/h2 = 4, \quad T_{UpperW} = 30°C, \quad (\partial T/\partial y)_{LowerW} = 0, \quad T_{inlet} = 20°C, \quad T_{outlet} = 20°C$

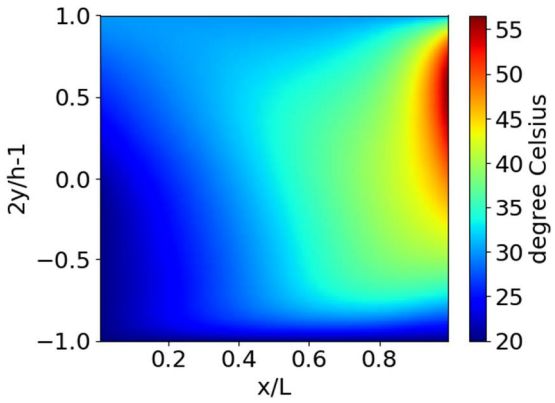

Figure A9: LPCM, $N_{Lobatto}$=10

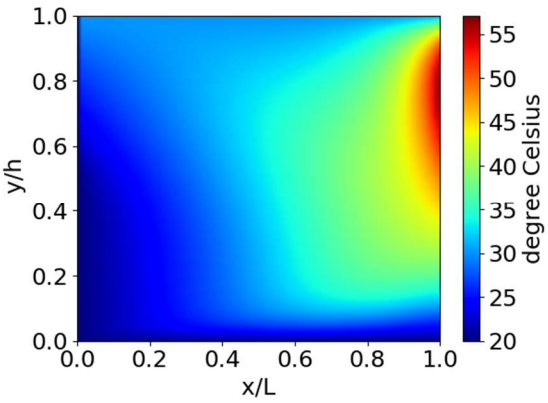

Figure A10: NDM, N_y=160

$h1/h2 = 4, \quad T_{UpperW} = 30°C, \quad T_{LowerW} = 20°, \quad T_{inlet} = 20°C, \quad T_{outlet} = 20°C$

References

1. Frêne, J. ; Nicolas, D. ; Degueurce, B. ; Berthe D. and Godet M. "Lubrification hydrodynamique- paliers et butées", Paris: Eyrolle, France 1990 ; ISBN-13 : 978-2212016208
2. Elrod, H.G.; Brewe, D.E. "Thermohydrodynamic Analysis for Laminar Lubricating Films," NASA Technical Memorandum No. 88845, 1986.
3. Elrod, H.G. "Efficient Numerical Method for Computation of the Thermohydrodynamics of Laminar Lubricating Films," ASME J. Tribol., 1991, 113(3), pp. 506–511, DOI:10.1115/1.2920652
4. Moraru, L."Numerical Predictions and Measurements in the Lubricationof Aeronautical Engine and Transmission Components," Ph.D. thesis, The University of Toledo, OH, pp. 157–159, 2005
5. Feng, K.; Kaneko, S. "Thermohydrodynamic Study of Multiwound Foil Bearing Using Lobatto Point Quadrature", ASME. J. Tribol., 2009, DOI: 10.1115/1.3070579
6. Mahner, M.; Lehn A. and Schweizer B., "Thermogas- and thermohydrodynamic simulation of thrust and slider bearings: Convergence and efficiency of different reduction approaches", Tribology International, Volume 93, Part B, Pages 539-554, 2015, DOI: 10.1016/j.triboint.2015.02.030
7. Ferziger, J.H.; Peric, M. "Computational Methods for Fluid Dynamics", third, rev. edition, Springer, 2002, ISBN: 978-3-319-99693-6

8. Giraudeau, C.; Bouyer, J.; Fillon, M.; Hélène, M. and Beaurain, J. "Experimental Study of the Influence of Scratches on the Performance of a Two-Lobe Journal Bearing", Tribology Transactions, 2016, DOI: 10.1080/10402004.2016.1238528
9. Elrod, H.G. "A cavitation algorithm", ASME J. Tribol., 1981, Vol. 103, pp.350-354, DOI: 10.1115/1.3251669
10. Bonneau, D. ; Fatu, A. ; Souchet, D. "Paliers hydrodynamiques1 and 2, équations, modèles numériques isothermes et lubrification mixte", Lavoisier, Paris, 2011, ISBN 978-2-7462-3299-0
11. Woloszynski, T.; Podsiadlo, P.; Stachowiak, G.W. "Efficient Solution to the Cavitation Problem in Hydrodynamic", Tribology Letters, Springer, 2015, DOI: 10.1007/s11249-015-0487-4